Bulletin of Earth Sciences of Thailand

Micro-CT Imaging for Shale Pore Networks from Huai Hin Lat Formation

Punnaya Lertsrisunthad* and Piyaphong Chenrai
M.Sc. Petroleum Geoscience Program, Department of Geology, Faculty of Science, Chulalongkorn University, Bangkok, 10330, Thailand
*Corresponding author e-mail: PunnayaL@pttep.com

Abstract

Shale gas has emerged as a significant energy resource globally due to its abundance, cost-effectiveness, and environmental advantages. Understanding the geological and physical properties of shale formations, particularly porosity, is crucial for optimizing production and recovery rates. This study focuses on investigating the porosity characteristics of mudstone samples from the Sap Phlu Basin and the Na Po Song Basin in Thailand's Huai Hin Lat Formation, a potential shale gas prospect. Micro computed tomography (micro-CT), X-ray fluorescence (XRF), and X-ray diffractometer (XRD) techniques were employed to analyze the porosity and mineral composition of the samples. The results revealed distinct differences in porosity between the two basins, with porosity levels ranging from 0.05% to 0.07% in the Sap Phlu Basin and 0.12% to 0.17% in the Na Po Song Basin. The dominant mineral composition, primarily calcite, contributed to denser matrices and potentially lower porosity. However, the presence of quartz, albite, and dolomite influenced porosity variations within the samples. Fracture porosity, observed particularly in samples cut parallel to the bedding plane, highlighted its beneficial role in enhancing fluid flow within the mudstone formations, indicating its potential significance in shale gas extraction. These findings provide valuable insights into the porosity characteristics, mineral composition, and fracture porosity dynamics in mudstone reservoirs, essential for assessing shale gas reservoir potential and informing production strategies.

Keywords: Micro computed tomography, Huai Hin Lat Formation, Sap Phlu Basin, Na Po Song Basin, Porosity

1. Introduction

Shale gas has become an increasingly important energy resource worldwide due to its abundance, low cost, and environmental advantages over traditional fossil fuels (Meakin, 2013). To produce hydrocarbons from shale gas, it is essential to understand its geological, physical, and chemical properties, particularly its porosity. Porosity is the measure of the amount of empty space within a rock. In shale formations, porosity is typically very low due to tight packing of clay particles. However, natural fractures and other permeable pathways can enhance porosity and improve productivity of shale gas (Walton and McLennan, 2013). Thus, porosity in shale gas is crucial for optimizing production and improving recovery rates.

There are several shale gas prospects in Thailand such as the Dat Fa Member in the Huai Hin Lat Formation (Figure 1; Schenk et al., 2017; Chenrai et al., 2022).

The Huai Hin Lat Formation is known as a potential source of unconventional hydrocarbons with high organic content (Chenrai et al., 2022). The geological properties

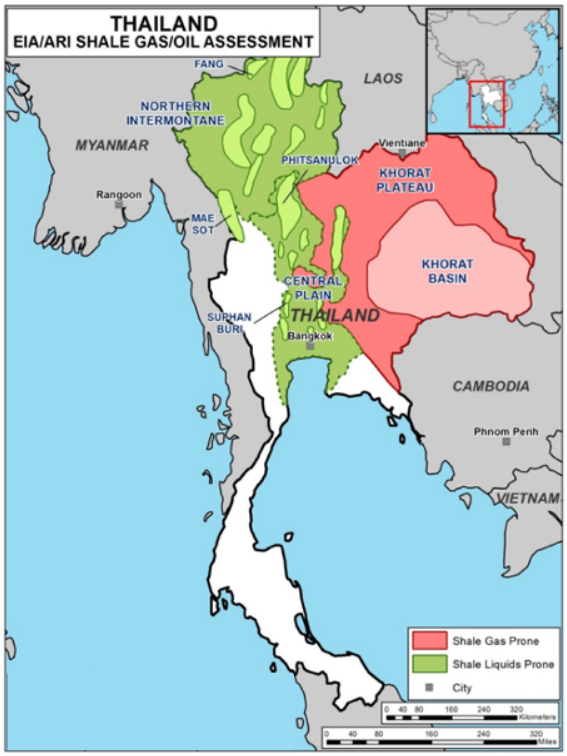

Figure 1 Prospective shale gas and shale oil basins of Thailand (modified from Advanced Resource International, 2013).

of the Huai Hin Lat Formation indicate that it has a good unconventional reservoir potential, with high total organic carbon content and favorable thermal maturity levels (Sattayarak et al., 1989).

Thus, this study aims to investigate the porosity of the shale gas in the Huai Hin Lat Formation in Thailand using micro computed tomography (micro-CT), X-ray fluorescence (XRF) and X-ray diffractometer (XRD) techniques to better understand its storage potential and optimize production parameters.

This study utilized four samples from the Huai Hin Lat Formation in the Sap Phlu Basin and the Na Po Song Basin. The samples consist of two samples of mudstone collected from the Dat Fa members in the Sap Phlu Basin (SPM) and two samples of calcareous mudstone collected from the Na Po Song Basin (NPM) as shown in **Figure *1***.

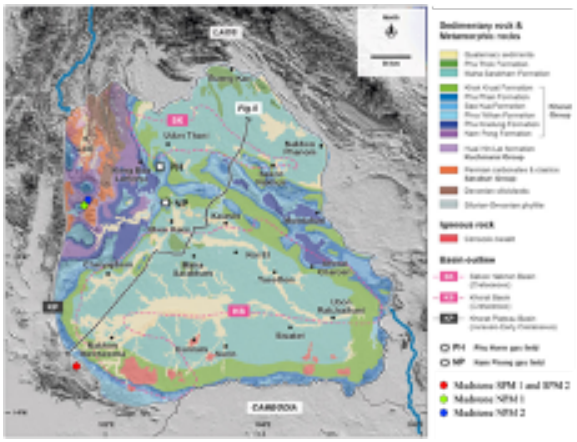

Figure 1 Sample locations with geological map of the study area (modified from Chenrai et al., 2022)

2. Geological Setting

The Huai Hin Lat Formation is located in the Khorat Plateau, northeastern Thailand (Figure 1 andFigure **3**). The Formation consists of mudstone, sandstone, and conglomerate that were deposited during the Late Triassic (Norian) age based on the *Estheria* fauna, spores, and pollen (Haile,1973; Kobayashi,1973; Konno and Asama, 1973; Chonglakmani and Sattayarak, 1978).

The Khorat Plateau is a complicated system of basins formed by extension in the

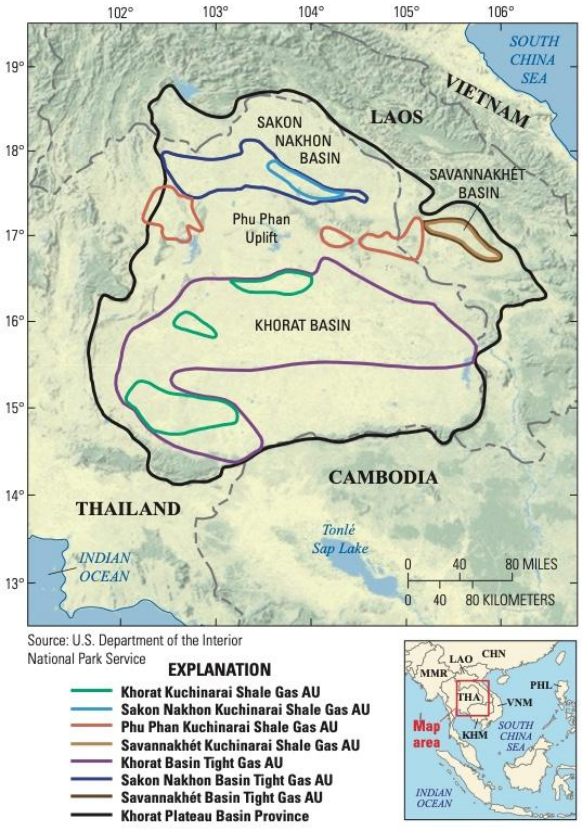

Figure 3 Map showing the recoverable shale-gas and tight-gas resources in the Khorat Plateau, Thailand and Laos (Schenk et al., 2017)

Late Triassic period and filled with sediment dominated by fluvial processes (Cooper, 2000). These basins formed about 200 million years ago, following a period of compressional stress caused by the collision of the Shan-Thai terrane with the rest of Indochina (Figure 4). This event of extension in the Triassic period is thought to be related to the collapse of the earth's crust, which had become overly thickened due to the compressional phase of the Indosinian orogeny. This transition from compression to extension happened quickly and was likely influenced by the introduction of magma that weakened the lithosphere. The basins in northeast Thailand were formed during this period and were primarily controlled by pre-existing structural

features and the distribution of underlying strata (Chonglakmani and Sattayarak, 1978). The Jurassic and Cretaceous rocks of the Khorat mega-sequence were deposited after the Triassic period and were subject to thermal subsidence. Later, in the Late Cretaceous and Early Tertiary periods, the Triassic basins were inverted, developing extensive, large-scale structures in and around the margins of the Khorat Plateau.

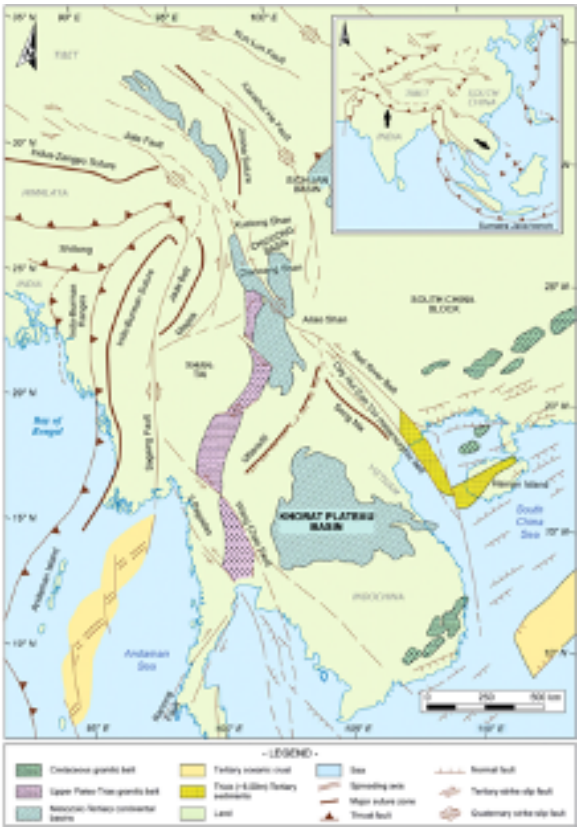

Figure 4 Southeast Asia Structural framework map (HIS, 2023). Modified after Searle, (2006).

The Huai Hin Lat Formation was formed in areas known as half-grabens and was mainly composed of mudstone, sandstone, and conglomerate layers that were deposited from alluvial fan, restricted lacustrine and fluviatile facies (Figure A; Chenrai et al, 2022; Chonglakmani and Sattayarak, 1978).

The Huai Hin Lat Formation is visible at the edge of the Khorat Plateau and is situated beneath the Khorat Group, which ranges from the Late Cretaceous to Rhaetian age, in sub-surface basins. The primary source rock of Huai Hin Lat for oil and gas in the basin is believed to be the lacustrine mudstones that formed during the Triassic period (Christopher, 2011).

The Huai Hin Lat Formation has thickness around 400 meters. It is situated below the Permian and older rock formations with an uncon formity, and it is covered by the Nam Phong Formation with another unconformity. The Huai Hin Lat Formation consists of five different units, which are the PhoHai, Sam Khaen Conglomerate, Dat Fa, Phu Hi, and I Mo Members. These units are arranged in a sequential manner from the bottom to the top. (Figure B; Chonglakmani and Sattayarak, 1978).

1) I Mo Member: of grey sandstone, shale and limestone with associated intermediate volcanic rocks.
2) Phu Hi Member: of grey sandstone, shale and argillaceous limestone with some intercalations of conglomerate beds.
3) Dat Fa Member: of grey to black c arbonaceous, calcareous, well-bedded shale and argillaceous limestone. It contains both flora and fauna indicating a Late Triassic (Norian) age.
4) Sam Khaen Conglomerate Member: chiefly of conglomerate with some intercalations of finer sediments. It is mainly a lateral equivalent of the Pho Hai Member, but locally overlies it.
5) Pho Hai Member: mainly tuff, agglomerate, rhyolite and andesite with some intercalations of sandstone, mudstone.

3. Materials and Methods

This study focuses on the rock properties of the mudrock from the Dat Fa member of the Huai Hin Lat Formations. Porosity determination was performed by using an integration of field investigation, image processing and geochemical analysis.

Small cylindrical samples with a diameter of 2-3 mm and length of 8-10 mm are commonly utilized in CT scanning to acquire high-resolution data. The process involves rotating the sample stage during scanning, which enables the X-rays to scan the core plug from multiple angles.

The process involves capturing a series of 2D images at various angles and reconstructing

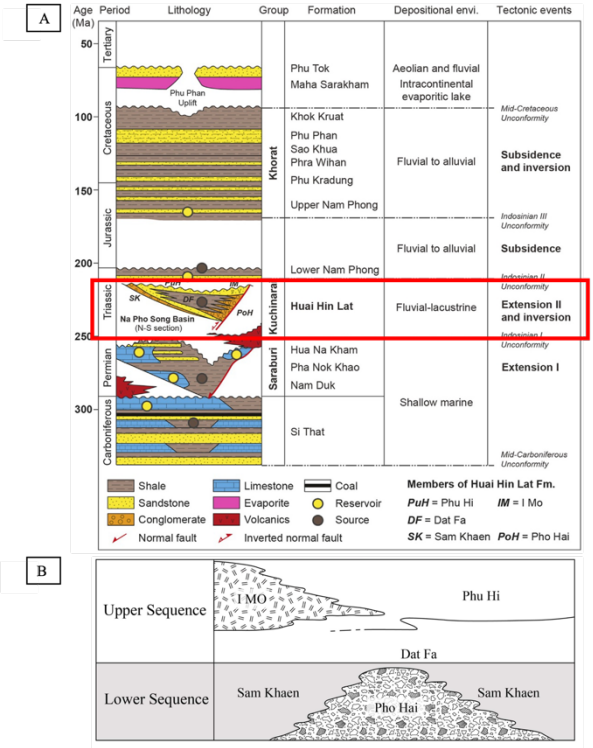

Figure 5 (A) Stratigraphy of the Khorat Plateau including petroleum system elements and key events (Chenrai et al, 2022). (B) The classified members of the Huai Hin Lat Formation (Chonglakmani and Sattayarak, 1978)

them into a 3D volume using specialized software, this study used Dragonfly software. Before reconstruction, the raw images undergo image processing, including denoising, filtering, segmentation, and binarization, to remove defects and extract the target object, which includes the pore space and mineral composition. By thresholding the grey-scale values in the 3D volume, different pore sizes or types can be highlighted. Once the pore space is segmented, various pore network analysis techniques can be used to quantify the pore structure of samples. The general workflow of the model reconstruction including image processing is illustrated in Figure .

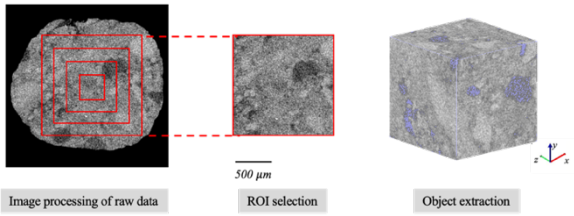

Figure 6 Image processing and pore space extraction. The red square box donates different size of calculation domains; and the gray cubic model represents the pore phase and grain phase, respectively.

4. Results

4.1 Major mineral composition

Table 1 shows the detailed mineral compositions from XRD data from the samples. The mineral components are dominated by calcite (30.64–87.63 wt %, average 68.80 wt %) and quartz (2.12–33.91 wt %, average 15.22 wt %) followed by feldspar (albite) (0-20.88 wt %, average 9.03 wt %). Dolomite, 36.02 wt %, was only detected from only sample NPM 2.

Sample no.	SPM 1	SPM 2	NPM 1	NPM 2
Quartz	12.37	33.91	2.12	12.46
Calcite	87.63	64.55	92.40	30.64
Dolomite	-	-	-	36.02
Albite	-	1.54	5.48	20.88
Total	100.00	100.00	100.00	100.00

Table 1 Mineral assemblages of the rock samples from the Huai Hin Lat Formation. Noted that SPM = Sap Phlu mudstone and NPM = Na Po Song mudstone.

4.2 Major element geochemistry

Significant variations can be observed in the major element concentrations in the samples (Table 2). CaO and SiO_2 concentrations in the samples varied from 18.24 to 73.60 wt% with an average of 48.86 wt% and 17.78 to 45.88 wt% with an average of 35.45 wt%, respectively.

Wide variations were also observed in Al_2O_3 (0.90-11.29 wt%), MgO (1.39-11.39 wt %), and K_2O content (0.30-2.71wt%) with an averages of 5.62 wt%, 5.05 wt%, and 1.13 wt%, respectively. The Fe_2O_3 (iron) concentrations in the samples varied from 0.69 to 5.98 wt% with an average of 2.25 wt%. Sodium (Na) concentrations are low in Sap Phlu mudstone samples compared to Na Po Song mudstone samples (Table 2). The Na contents in Na Po Song mudstones reflect the presence of plagioclase (albite) (Tables 1 and 2).

The most abundant elements are calcium (Ca), silicon (Si), aluminum (Al), magnesium (Mg), and iron (Fe) (Table 2). Silicon is mainly associated with quartz and clay minerals in fine-grained sediments (Fu et al., 2010a; Fu et al., 2010b; Zeng et al., 2015). Thus, the Si/(Si + Al + Fe) ratio can be used to indicate the terrigenous provenance distance in which the ratio decreases with the increasing distance (Li et al., 2018). The Si/(Si + Al + Fe) ratio of the samples varies from 0.73 to 0.94 with an average of 0.83 (Table 2), and indicates that the samples were deposited near terrigenous provenance (Chenrai et al., 2022).

Sample no.	SPM 1	SPM 2	NPM 1	NPM 2
CaO	69.50	34.11	73.60	18.24
SiO_2	26.33	51.80	17.78	45.88
Al_2O_3	0.90	5.89	4.41	11.29
Fe_2O_3	0.69	1.58	0.76	5.98
MgO	1.64	5.76	1.39	11.39
Na_2O	0.00	0.08	0.70	4.16
K_2O	0.30	0.58	0.93	2.71
TiO_2	0.00	0.06	0.00	0.25
P_2O_5	0.66	0.12	0.42	0.08
Total	100.02	99.99	100.00	99.97

Table 2 Major element data of the rock samples from the Huai Hin Lat Formation. Noted that SPM = Sap Phlu mudstone and NPM = Na Po Song mudstone.

The Huai Hin Lat Formation was examined by analyzing four mudstone samples using the x-ray microtomography technique. Eight small cylindrical samples were obtained by cutting them from four mudstone samples (SPM 1, SPM 2, NPM 1 and NPM 2). Each rock sample was cut both perpendicular and parallel to the bedding plane.

4.3 2D Image Analysis

Porosity images of the samples are processed by Dragonfly software. To handle the large amount of digital data per sample, the samples were randomly divided into smaller cubes in the software, enabling quicker 3D segmentation and processing. These smaller cubes, referred to as volumes of interest (VOIs), are 1500 x 1500 x 1500 μm^3 and provide porosity's geometry and distribution.

The x-ray microtomography technique was employed to generate 2D reconstruction images, as certain micro-scale features were more readily observable and distinct in high-resolution 2D images. The XY, XZ, and YZ planes of the volumes of interest (VOIs) were utilized to extract basic features for quantitative analysis. These features encompassed pore, kerogen, and pyrite within the VOIs, and their visible geometry, size, and distribution were characterized. Figure displays examples of 2D images.

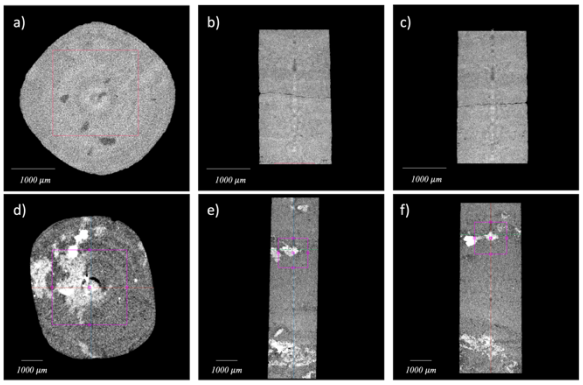

Figure 7 Examples of 2D reconstruction images:(a), (b), and (c) from Mudstone SPM 1 perpendicular in XY, XZ and YZ planes, respectively, and (d),(e), and (f) from Mudstone NPM 2 perpendicular in XY, XZ and YZ planes, respectively.

The features observed in the 2D analysis are expected to be significant indicators

influenced by factors such as compaction, burial depth, and maturation. According to Loucks et al. (2012), these features are categorized as different types of pores, including interparticle pores, intraparticle pores, organic-matter pores, and fracture pores (microcracks) (**Figure**). Bedding-parallel cracks were observed in samples SPM 1.

Intraparticle pores were mainly observed within mineral framboids from NPM 1 and NPM 2 (Fig. 9 and 10). Organic-matter pores were clearly visible in SPM 1 (Figure).

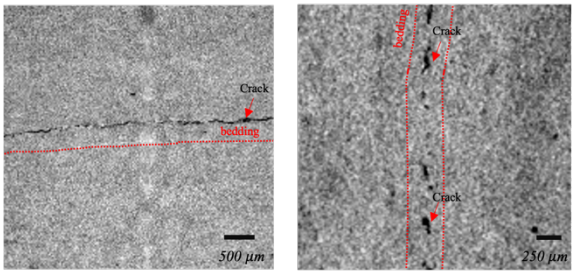

Figure 8 2D images of SPM 1 perpendicular to the bedding (left) and parallel to the bedding (right) show fracture pores (crack) that are parallel to the bedding of the sample.

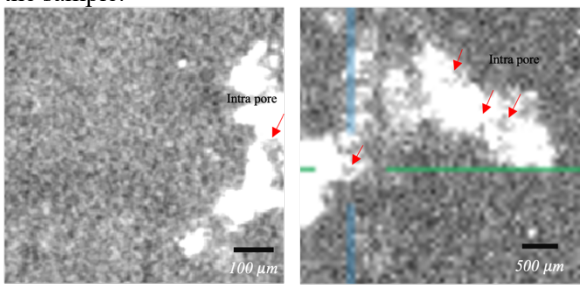

Figure 9 2D images of NPM 1 parallel to the bedding show intraparticle pores within mineral framboids.

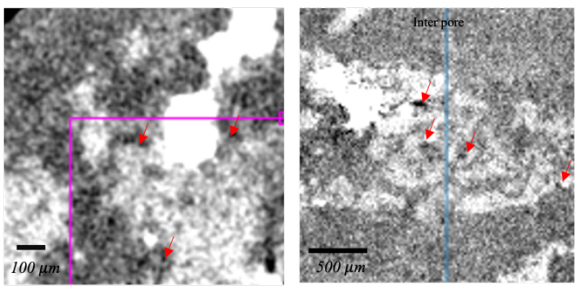

Figure 10 2D images of SPS 2 (left) and NPM 2 (right) perpendicular to the bedding show interparticle pore between grains.

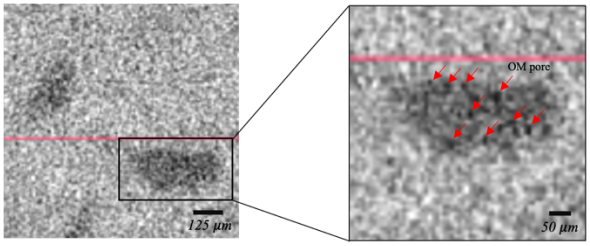

Figure 11 Organic-matter pores are observed from SPM 1 perpendicular to the bedding.

4.4 Porosity Analysis of Mudstone Samples Using Micro CT

Micro-CT imaging technique was employed to assess the porosity of the mudstone samples accurately and non-destructively. The technique provides high-resolution images and quantification of the pore spaces within rock samples. The porosity characteristics of the mudstone samples (SPM 1, SPM 2, NPM 1, and NPM 2) were examined in both perpendicular and parallel orientations to the bedding plane.

In SPM 1, the perpendicular orientation exhibited a porosity of 0.05%, primarily consisting of small-sized organic matter pores (Figure a). On the other hand, the parallel orientation showed a slightly higher porosity of 0.06%, characterized by an abundance of small-sized pores and the presence of medium and large fracture pores (Figure b).

The perpendicular orientation from SPM 2 yielded a consistent porosity of 0.05%, with a varied distribution of pore sizes and diverse sphericity (Figure c). In the parallel orientation, the porosity increased to 0.07%, accompanied by a varied pore size distribution, with medium-sized pores being predominant, and the presence of fracture pores contributing to the complexity of pore shapes (Figure 11d).

NPM 1 revealed a higher porosity of 0.14% in the perpendicular orientation, characterized by interparticle, intraparticle, and small-sized organic matter pores (Figure e). In the parallel orientation, the porosity further increased to 0.17%, with porosity concentration

observed in small-sized pores, along with a spike indicating the presence of larger-sized fracture pores (Fig. 11f).

Lastly, the perpendicular orientation from NPM 2, exhibited a porosity of 0.10%, with a significant occurrence of small-sized pores and the presence of medium and large-sized interparticle, interlayer, and fracture pores (Fig. 11g). Similarly, the parallel orientation displayed a porosity of 0.10%, with the presence of small to medium-sized pores (Fig. 11h).

5. Discussions

5.1 Porosity between the Sap Phlu Basin and the Na Po Song Basin

The analysis of porosity using micro-CT scanning revealed variations in porosity values among Mudstone Samples (SPM 1, SPM 2, NPM 1 and NPM 2) as showed in **Figure** . The samples from the Sap Phlu Basin exhibited porosity ranging from 0.05% to 0.07%, while the samples from the Na Po Song Basin displayed higher porosity values ranging from 0.12% to 0.17%. These variations suggest distinct differences in the amount of void spaces within the mudstone samples between the two basins Possible factors such as mineral composition, grain size, and the presence of fractures or vuggy structures may affect the differences in porosity values.

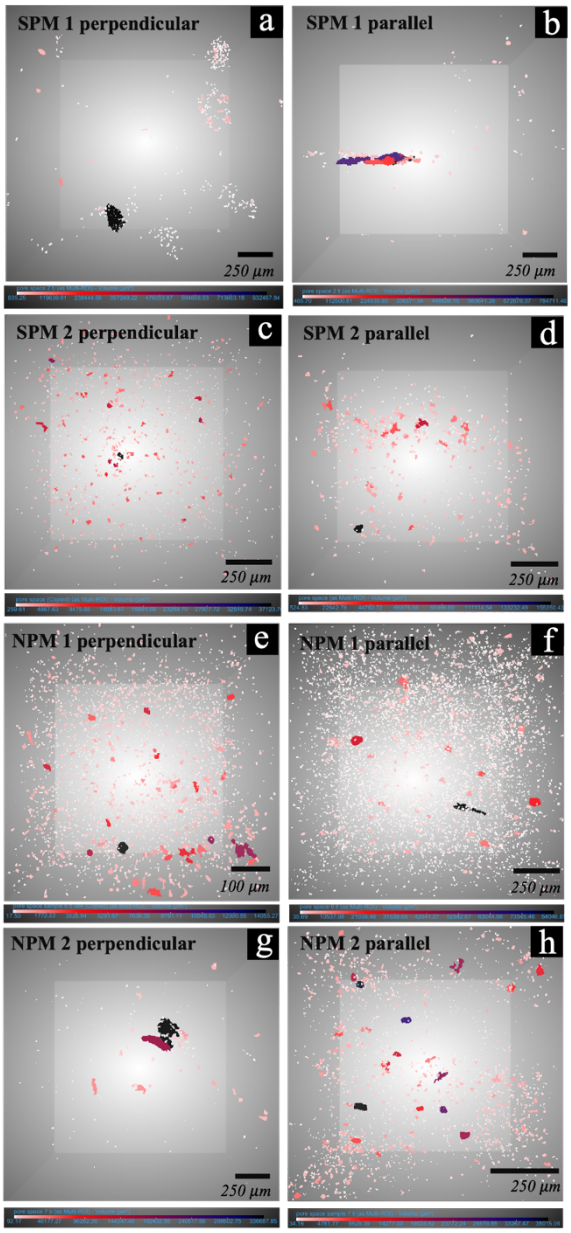

Figure 11 (a) to (h) Images illustrate spatial distribution of pores from the mudstone samples SPM 1, SPM 2, NPM 1, and NPM 2 with shading corresponding to their size. Notably, each sample was examined both perpendicular and parallel to the bedding plane.

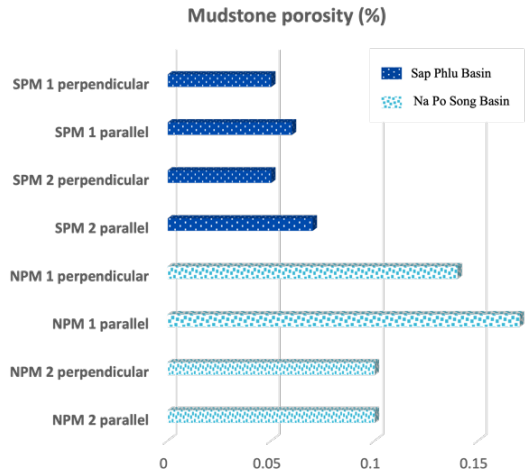

Figure 12 Comparison of porosity between the Sap Phlu Basin and the Na Po Song Basin.

5.2 Porosity between parallel and perpendicular to bedding

The utilization of parallel bedding plane cutting enhances the clarity of observing fracture pores compared to perpendicular cuts. The analysis of porosity in the mudstone samples demonstrated varying characteristics in both perpendicular and parallel orientations. The perpendicular orientations generally exhibited lower porosity values, with variations in pore size distribution and the presence of different types of pores, including organic matter pores and interparticle pores. Conversely, the parallel orientations generally displayed slightly higher porosity values, with the prevalence of small to medium-sized pores and the significant occurrence of fracture pores contributing to the overall porosity. These findings highlight the complex nature of porosity in mudstone reservoirs and emphasize the importance of considering both pore size distribution and fracture porosity when evaluating their potential for fluid storage and flow (e.g., Yao et al., 2020).

This suggests that fracture porosity may play a beneficial role in fluid flow within the rock formation and could potentially serve as a parameter for hydraulic fracturing operations in oil production. Additional research and data could further explore the significance of fracture porosity and its implications for fluid flow dynamic and reservoir stimulation.

5.3 Relationship between mineral composition and porosity

The porosity within the Sap Phlu Basin, consisting of SPM 1 and SPM 2, shows a relatively similar range of 0.05% to 0.07%. Both samples are dominated by calcite, suggesting a denser matrix and potentially lower porosity. However, the presence of quartz contributes to some porosity, with SPM 2, having a higher quartz content, likely exhibiting slightly higher porosity compared to SPM 1. The minor presence of albite in SPM 2 has minimal influence on the overall porosity.

In contrast, the porosity within the Na Po Song Basin, consisting of NPM 1 and NPM 2, varies within the range of 0.10% to 0.17%. Both samples exhibit a significant presence of calcite, indicating a denser matrix and potentially lower porosity. However, NPM 1 demonstrates relatively higher porosity due to its lower calcite content and the presence of small amounts of quartz and albite. NPM 2, on the other hand, has lower porosity attributed to its higher calcite content and the significant presence of dolomite, further contributing to the denseness of the sample.

Thus, the presence of quartz in shale samples may increase porosity within shale gas formation (e.g., Buntoro et al 2018; Iqbal et al. 2021; Wang et al., 2023).

6. Conclusions

The analysis of porosity in mudstone samples from the Sap Phlu Basin and the Na Po Song Basin revealed distinct differences in porosity characteristics. The samples from the Sap Phlu Basin exhibited porosity levels ranging from 0.05% to 0.07%, while the samples from the Na Po Song Basin displayed higher porosity values ranging from 0.12% to 0.17%. These variations suggest different levels of void spaces within the mudstone samples, indicating their

potential for fluid storage and flow. The mineral composition played a significant role, with the dominant calcite composition in both basins contributing to a denser matrix and potentially lower porosity. However, the presence of quartz in the Sap Phlu Basin resulted in slightly higher porosity in the samples. The findings highlight the importance of considering mineral composition in assessing porosity characteristics in mudstone reservoirs.

The presence of fracture pores, particularly in the samples cut parallel to the bedding plane increase porosity in the samples. This suggests that fracture porosity may play a beneficial role in fluid flow within the mudstone formations, particularly in the context of shale gas extraction.

7. Acknowledgements

The expertise and assistance provided by the Micro-CT lab staff were crucial in conducting the micro-CT imaging and analysis. I am also grateful to all those who have contributed in any way to this paper, especially Wongsakorn Choowala who is a platinum field assistant. Lastly, I extend my deepest appreciation to my family, friends, and loved ones for their unwavering support.

8. References

Buntoro, A., Prasetyadi, C., Wibowo, R., Ahamd Muraji, S. & Haryanto, A. 2018. Validation of shale brittleness index calculation from wireline log of well BETRO-001 by using XRD test results and uniaxial test as parameters for determining the potential of shale hydrocarbon - brown shale of Pematang Group Formation, Central Sumatra Basin, Bengkalis Trough. *IOP Conference Series: Earth and Environmental Science*, 212, 012069

Chenrai, P., Jitmahantakul, S., Bissen, R. & Assawincharoenkij, T. 2022. A preliminary assessment of geological CO2 storage in the Khorat Plateau, Thailand. *Frontiers in Energy Research*. 10:909898.

Chonglakmani, C. & Sattayarak N 1978. Strigraphy of the Huai Hin Lat Formation (Upper Triassic) in northeastern Thailand. *Proceedings on the Third Conference on Geology and Mineral Resources of Southeast Asia*. Bangkok, 739–762.

Cnudde, V. & Boone M.N. 2013. High-resolution X-ray computed tomography in geosciences: A review of the current technology and applications. *Earth-Science Reviews*, 123, 1-17. ISSN 0012-8252.

Schenk, C. J., Klett, T. R., Mercier, T. J., Finn, T. M., Tennyson, M. E., Gaswirth, S. B., Marra, K. R., Le, P. A. & Drake II, R. M. 2017. Assessment of Continuous Gas Resources in the Khorat Plateau Province, Thailand and Laos, 2016. US Geological Survey.

Fu, X., Wang, J., Zeng, Y., Tan, F., Chen, W. & Feng, X. 2010a. Geochemistry of rare Earth elements in marine oil shale - a case study from the Bilong Co area, Northern Tibet, China. *Oil Shale* 27, 194-208.

Fu, X., Wang, J., Zeng, Y., Tan, F. & Feng, X. 2010b. REE geochemistry of marine oil shale from the Changshe Mountain area, northern Tibet, China. International Journal of Coal Geology, 81, 191-199.

Haile, N.S. 1973. Note on Triassic Fossil Pollen from Nam Pha Formation, Chulabhon (Nam Phrom) Dam, Thailand. *GST Newslett*, 6, 15-16.

Iqbal, M.A., Rezaee, R., Smith, G., & Ekundayo, J.M. 2021. Shale lithofacies controls on porosity and pore structure: An example from Ordovician Goldwyer Formation, Canning Basin, Western Australia. *Journal of Natural Gas Science and Engineering*, 89, 103888.

Kobayashi, T. 1973. Upper Triassic estheriids in Thailand and the conchostracan development in Asia in Mesozoic Era. *Geology and Paleontology of Southeast Asia,* 16, 57-90.

Konno, E. & Asama, K. 1973. Mesozoic plants from Khorat, Thailand. *Geology and Paleontology of Southeast Asia*, 12, 149-172.

Li, D., Li, R., Xue, T., Wang, B., Liu, F., Zhao, B. & Zhao, D. 2018. Characteristic and geological implications of major elements and rare Earth elements of Triassic Chang 7 oil shale in Tongchuan City, Southern Ordos Basin (China). *Minerals*, 8, 157.

Loucks, R., Reed, R., Rupple, S. & Hammes, U. 2012. Spectrum of pore types and networks in mudrocks and a descriptive classification for matrix-related mudrock pores. *The American Association of Petroleum Geologist,* 6 (June 2012), 1071-1098.

Toker, M., Ediger, V. & Evans, G. 2011. Unstable Shelf-Margin Tectonics of NE-Corner of Mediterranean Region, the Cilicia-Adana Basin. *International Conference on Geology, Geotechnology and Mineral Resources of Indochina (GEOINDO 2011).* 1.12.2011-3.12.2011. Khon Kaen.

Vinegar, H.J. & Wellington, S.L. 1987. Tomographic imaging of three-phase flow experiments. *The Review of Scientific Instruments*, 58, 96–107.

Walton, I. & Mclennan, J. 2013. The Role of Natural Fractures in Shale Gas Production. *Effective and Sustainable Hydraulic Fracturing*, 327–356.

Wang, J., Lu, S., Zhang, P., Zhi, Q., & Huang, H. 2023. Pore Distribution Characteristics of Different Lithofacies Shales: Evidence from Scanning Electron Microscopy. *Processes*, 11, 1120.

Yao, W., Mostafa, S., Yang, Z., & Xu, G. 2020. Role of natural fractures characteristics on the performance of hydraulic fracturing for deep energy extraction using discrete fracture network (DFN). *Engineering Fracture Mechanics*, 230, 106962. ISSN 0013-7944.

Zeng, S., Wang, J., Fu, X., Chen, W., Feng, X., Wang, D., Song, C. & Wang, Z. 2015. Geochemical characteristics, redox conditions, and organic matter accumulation of marine oil shale from the Changliang Mountain area, northern Tibet, China. *Marine and Petroleum Geology*. 64, 203–221.